Investigation of metabolite correlates of CEST in the human brain at 7 T

Schmitz Abecassis, B.; Najac, C.; Plugge, J.; Osch, M.J.P. van; Ercan, E.

Received: 25 August 2023 | Revised: 5 December 2023 | Accepted: 23 December 2023

DOI: 10.1002/nbm.5104

RESEARCH ARTICLE

NMR IN BIOMEDICINE WILEY

Investigation of metabolite correlates of CEST in the human brain at 7 T

Bárbara Schmitz-Abecassis[1,2] | Chloé Najac[1] | Jaimy Plugge[1,3] | Matthias J. P. van Osch[1,2] | Ece Ercan[1,4]

[1]C.J. Gorter MRI Center, Department of Radiology, Leiden University Medical Center, Leiden, The Netherlands

[2]Medical Delta, Delft, The Netherlands

[3]Leiden Institute of Physics, Leiden University, Leiden, The Netherlands

[4]MR R&D, Clinical Science, Philips, Best, The Netherlands

Correspondence
Bárbara Schmitz-Abecassis, C.J. Gorter MRI Center, Department of Radiology, C3Q, Leiden University Medical Center, P.O. Box 9600, 2300 RC, Leiden, The Netherlands.
Email: b.schmitz_abecassis@lumc.nl

Funding information
Dutch Research Council (NWO) Talent Programme Veni, Grant/Award Number: 16862; Medical Delta Cancer Diagnostics 3.0 program

Abstract

Metabolite-weighted chemical exchange saturation transfer MRI can be used to indirectly image metabolites such as creatine and glutamate. This study aims to further explore the contrast of CEST at 2 ppm in the human brain at 7T and investigate the metabolite correlates of CEST at 2 ppm via correlations with magnetic resonance spectroscopy (MRS). Simulations were performed to establish the optimal acquisition parameters, such as total saturation time (t_{sat}) and B_1 root mean squared (B_1rms) for CEST at 2 ppm in the human brain. Parameters were validated via *in vitro* phantom studies at 7T using concentrations, pH and temperature comparable to what is found in the human brain. Finally, 10 healthy volunteers were scanned at 7T for comparison with MRS. Our results show that the optimal parameters to acquire CEST at 2 ppm images are: B_1rms = 2.14 μT & t_{sat} = 1500 ms, respectively. Comparison with MRS showed no significant correlation between CEST at 2 ppm and total Creatine measured by MRS (R = 0.19; *p*-value = 0.273). However, a significant correlation was found between CEST at 2 ppm and Glu (R = 0.39; *p*-value = 0.033), indicating the broad Glutamate-weighted CEST as the main measurable contributor to CEST at 2 ppm. We identified and confirmed optimal CEST at 2 ppm sequence parameters and validated CEST at 2 ppm measurements in a controlled *in vitro* environment. Our findings suggest that glutamate is a substantial contributor to the CEST at 2 ppm contrast observed in the human brain, whereas the creatine contribution to CEST at 2 ppm in the brain did not show a measurable contribution.

KEYWORDS
7 T, CEST at 2 ppm, human brain, metabolite-weighted CEST, MRS

Abbreviations: AREX, apparent exchange-dependent relaxation; B_1rms, B_1 root mean squared; CEST, chemical exchange saturation transfer; CRLB, Cramér–Rao lower bound; CSF, cerebrospinal fluid; Glu, glutamate; GM, gray matter; MT, magnetization transfer; MTR, magnetization transfer ratio; NOE, nuclear Overhauser effect; PCC, posterior cingulate cortex; SAR, specific absorption rate; t_{sat}, total saturation time; UHF, ultrahigh field; VOI, voxel of interest; WASSR, water saturation shift reference; WM, white matter.

1 | INTRODUCTION

Chemical exchange saturation transfer (CEST) MRI is an emerging technique that allows us to noninvasively image endogenous metabolites and proteins *in vivo*.[1] CEST is derived from the exchange of protons between the bulk water pool and the solute pool of interest. CEST contrast is achieved by applying a train of frequency specific RF pulses with a certain B_1 power to saturate the pool of interest and by measuring the decrease in the signal from the water pool due to chemical exchange. CEST is a very sensitive technique for *in vivo* metabolic imaging and greatly benefits from ultrahigh field (UHF) (e.g., 7, 9.4 T MRI), exploiting the advantage of higher signal-to-noise ratio and higher spectral resolution at UHF.

Fast and intermediate exchanging CEST pools of guanidium and amine protons, resonating at approximately 2 and 3 ppm from the water signal, respectively, have gained recent interest given the presence of these protons in metabolites such as creatine (Cr) and glutamate (Glu).[2] The most popular examples of metabolite-weighted CEST include Glu-weighted (CEST at 3 ppm) CEST for the brain and creatine-weighted (CEST at 2 ppm) CEST for brain and muscle.[3–6] The alteration of CEST at 3 ppm contrast from amine protons has also been investigated in the scope of brain pathologies. Especially in epilepsy, CEST at 3 ppm has shown promise in identifying epileptic foci in patients.[7] Similarly, in brain tumors, Neal et al. have shown increased CEST at 3 ppm in glioma-associated epilepsy, specifically in the peritumoral area.[8] CEST at 2 ppm, on the other hand, has mostly been explored for muscle imaging.[5] Preclinical work by Cai et al. has been able to correlate the concentration of Cr and CEST at 2 ppm contrast as an indicator of brain tumor aggressiveness.[9]

Differentiating between CEST at 2 ppm and CEST at 3 ppm pools in the brain can be challenging because of the proximity of their resonance spectra. While the exchange rates for CEST at 3 ppm and CEST at 2 ppm, and thus the optimal acquisition parameters for achieving maximum contrast, differ, other factors such as temperature and pH influence the resulting CEST effect.[10,11] The origins of CEST at 3 ppm are for the most part well established, despite a recent study suggesting that CEST at 3 ppm in the rat brain originates from amines in proteins.[12] Previous work has shown and validated the substantial contribution of Glu to CEST at 3 ppm contrast in the brains of a similar animal model and of three healthy volunteers.[13] However, limited work is available validating CEST at 2 ppm of the human brain *in vivo* at 7 T. The optimal acquisition parameters and metabolite correlates of CEST at 2 ppm in the human brain at 7 T are also yet to be established. Although Haris et al. have already investigated the feasibility of CEST at 2 ppm imaging in phantoms, this was not performed in the human brain at 7 T.[3] Singh et al. have carried out experiments at 7 T, evaluating the feasibility of CEST at 2 ppm imaging using *Z*-spectral fittings in phantoms as well as in a small group of four volunteers. However, phantom experiments did not include T_1 and T_2 corrections to match those of the brain, and the *in vivo* experiments did not include MRS validation to confirm the origins of CEST at 2 ppm or correlate the CEST at 2 ppm contrast with Cr concentration.[14]

The aim of this study is to further explore the CEST at 2 ppm contrast of the human brain and to investigate the metabolite correlates of CEST at 2 ppm through comparison with MRS measurements at 7 T. First, we simulated the CEST effect based on Bloch–McConnell equations to determine ideal B_1 and saturation time settings. Hereafter, we imaged phantoms made of Cr solutions to validate the optimized CEST acquisition parameters in vitro. Since CEST contrast is influenced by temperature, we also scanned a phantom at both room and body temperatures to determine to what extent this variation could influence the contrast obtained. Finally, we investigated metabolite correlates of CEST at 2 ppm of the human brain *in vivo* via comparison with MRS. To achieve this goal, we scanned 10 healthy volunteers using a 7 T human MRI system and examined the correlation between tCr obtained from MRS and CEST at 2 ppm. In contrast to previous studies,[10,12,13,15] we also assessed if Glu has makes a contribution to the CEST at 2 ppm contrast, given the broad effect of the CEST at 2 ppm pool, and the closely resonating CEST at 3 ppm pool. We further computed the apparent exchange-dependent relaxation (AREX) employing a multi-pool Lorentzian fitting of the *in vivo* data. This approach aimed to correct for competing CEST effects and T_1 scaling. The goal was to see if statistical results differed from those obtained using the conventional magnetization transfer ratio (MTR) asymmetry metric.

2 | METHODS

2.1 | Simulations

CEST from Cr in the human brain was simulated via Bloch–McConnell equations, using a five-pool model, including Cr, Glu, nuclear Overhauser effect (NOE), water, and magnetization transfer (MT) pools. The goal was to simulate the CEST MTR asymmetry when using different total saturation time (t_{sat}) and B_1 root mean squared (B_1rms) values, such that we could assess which parameter combination would yield maximum signal intensity. For each pool, we considered literature values of exchange rate constants for spontaneous (k_0) and base (k_b) catalysis (Cr, $k_0 = 0$ Hz and $k_b = 7.81{\cdot}10^9$ Hz; Glu, $k_0 = 2.79 \times 10^3$ Hz and $k_b = 4.5 \times 10^{10}$ Hz; NOE, $k_0 = 0$ Hz and $k_b = 16 \times 10^7$ Hz) as well as T_2 values at 7 T (Cr, 7.1 ms; Glu, 6.9 ms). Both metabolite concentrations were kept at 10 mM to mimic the approximate conditions in the human brain. For water, T_1 and T_2

were 1.6 s and 62 ms respectively. Finally, MT was simulated as a semisolid pool given the very short T_2 times ($\pm 10^{-5}$ s), thus we only considered its Z-magnetization.[16]

2.2 | Phantom preparation

First, a phantom was prepared consisting of 10 vials of 60 mL each, which were placed in a glass container with Electronic Liquid FC-3283 (Fluorinert, 3M), embedding the tubes: (1) deionized water only, (2) a mixture of Cr (10 mM) and Glu (10 mM), (3–10) Cr or Glu with a range of concentration from 5 to 40 mM. Cr and Glu phantoms were made with *N*-amidinosarcosine and L-glutamic acid, respectively. Our objective was to establish a gradient of concentrations for the two metabolites, incorporating levels that closely approximate *in vivo* concentrations in the brain. Additionally, higher concentrations were included to evaluate the correlation between CEST and metabolites' concentration. Ultimately, the phantom was scanned at room temperature (21.5 °C), at approximately 28 °C, and finally at 36 °C. The goal was to create a temperature gradient to observe how the CEST contrast would change as a function of temperature. Second, we prepared an additional phantom with four vials of 50 mL each. The goal was to match the metabolite concentration and correct for T_1 and T_2 relaxation times found in the human brain. These vials contained (1) deionized water, (2) 10 mM Cr and 10 mM Glu, (3) 10 mM Cr and (4) 10 mM Glu, a range of concentration similar to those in previous studies.[3] A total of 0.5 mM $CuSO_4$ and 1% agarose were added for T_1 and T_2 adjustments.[17] Initial optimization of $CuSO_4$ and 1% agarose concentrations showed no significant contributions of these compounds to the Z-spectra, except for an expected slight MT effect (Figure S4). All vials were titrated to achieve a physiological pH of approximately 7.3 (±0.05). Both phantoms were first heated to the desired temperature on a hot plate, then transferred into the scanner. To maintain the temperature constant while scanning, a water-circulating blanket was placed around the phantom container and connected to a Blanketrol III hyper–hypothermia system (Cincinnati Sub-Zero, Cincinnati, OH, USA). The temperature was monitored during image acquisition with an MRI compatible thermometer probe immersed in the Electronic Liquid FC-3283 or Fomblin perfluoropolyether (PFPE) medium surrounding the phantom tubes.

2.3 | *In vivo* data collection

We included 10 healthy volunteers (eight females, two males; 31.7 ± 16 years). The study adhered to the local institutional review board guidelines and approval. All participants gave written informed consent.

MRI scans were acquired using a whole body 7 T Philips Achieva MRI scanner (Philips Healthcare, Best, The Netherlands) equipped with a dual-transmit and a 32-channel receiver head coil (Nova Medical, Wilmington, MA, USA).

The acquisition protocol included a short survey scan, a sensitivity encoding (SENSE) reference scan, a B_0 map for third order B_0 shimming, a dual refocusing echo acquisition mode (DREAM) B_1 map to assess B_1 distribution and a water saturation shift reference (WASSR) scan for post-processing B_0 correction.[18] For B_1 inhomogeneity mitigation, we placed two dielectric pads on the right and left sides of the head. The dielectric pads were custom made as previously described by Teeuwisse et al.[19,20]

2.3.1 | CEST

The CEST imaging acquisition protocol was based on the outcome of the simulation and phantom studies and consisted of two CEST scans. First, to achieve an optimal CEST at 2 ppm contrast, a pulsed CEST preparation of 20 sinc–Gauss pulses of 50 ms with 25 ms interpulse delay (t_{sat} of 1500 ms) and a B_1rms of 2.14 μT was applied. Second, a pulsed CEST preparation of 20 sinc–Gauss pulses of 40 ms with no interpulse delay (t_{sat} of 800 ms) and a B_1rms of 3.3 μT was used to achieve an optimal CEST at 3 ppm contrast. In contrast to previous Glu-CEST experiments that were all performed with the same human 7 T platform from a different vendor and predominantly on one site, the interpulse delays used in our work were required to adhere to specific absorption rate (SAR) and RF amplifier requirements of the scanner used in our study. A total of 22 frequencies were acquired with a step size of 136.4 Hz between −1500 and 1500 Hz. CEST acquisition details regarding the scans initially performed in phantoms for optimization can be found in Table S1.

2.3.2 | MRS

The MRS acquisition protocol consisted of a short semi-LASER scan with a T_E of 34 ms and T_R of 6000 ms, 32 single acquisitions and a B_1 amplitude of 18 μT. Water suppression was achieved using the variable pulse power and optimization relaxation delays (VAPOR) sequence. Frequency offset corrected inversion (FOCI) refocusing pulses were used to minimize in-plane chemical shift displacement errors. In total, four voxels of

interest (VOIs) were acquired with dimensions 30 × 15 × 25 mm^3. VOIs were placed (1) in the frontal and posterior cingulate cortex (PCC) to maximize gray matter (GM) content and (2) in the left and right parietal white matter (WM) to maximize WM content, with effort to minimize the partial volume effect. A visual representation of the VOI planning can be found later in Figure 3. For each VOI, a separate water reference scan was acquired (same acquisition parameters, two single acquisitions).

2.4 | Data analysis

2.4.1 | Anatomical images

3D T_1-weighted images were segmented into probabilistic tissue maps for WM, GM and cerebrospinal fluid (CSF) using the FMRIB (Oxford Center for Functional Magnetic Resonance Imaging of the Brain) Software Library (FSL: Brain Extraction Tool and FAST algorithm).[21,22] A custom-built MATLAB routine was then used to create binary tissue maps (values are either 0 or 1, with 1 assigned to the tissue with highest probabilistic value) and quantify the volume of each tissue type within each MRS VOI. Maps were also used to mask CEST images to account only for voxels with GM and WM content above 70% (and thus limit partial volume effect).

2.4.2 | CEST

The WASSR data were used for B_0 inhomogeneity correction. B_1 corrections were made according to the method previously described.[23] The normalized, B_0 and B_1 corrected CEST images were then used to separately calculate the MTR asymmetry for 2 and 3 ppm CEST pools: $\mathrm{MTRasym} = \frac{Z(-x\ \mathrm{ppm}) - Z(+x\ \mathrm{ppm})}{Z(-x\ \mathrm{ppm})}$. We also fitted the data voxel wise to a five-pool Lorentzian model using the Levenberg–Marquardt algorithm.[24] More details can be found in the Supporting Information. AREX was calculated per voxel as described in a previous publication.[25]

The VOIs used for MRS acquisitions were used as masks to retrieve the CEST MTR asymmetry values.

2.4.3 | MRS

Water-suppressed MRS spectra were corrected for eddy currents and individual phase and frequency drift using a custom-built MATLAB routine and fitted with LCModel.[26] A basis-set was generated using the FID-A toolbox.[27] Non-water-suppressed data from the same VOI were used for quantification. The water signal was corrected for GM, WM and CSF tissue fractions. Literature values for T_1 and T_2 relaxation time values of water in GM, WM and CSF as well as T_1 and T_2 relaxation time values of neurometabolites were used for correction.[28] Cramér-Rao lower bounds (CRLBs) for total creatine (tCr = Cr + PCr) and Glu were obtained from LCModel output. Individual water acquisitions were inspected for any large phase or amplitude drop (which could be explained with subject movement). For one dataset in the PCC we observed a large phase change in one of the single acquisitions and excluded it before averaging all other single acquisitions.

2.5 | Statistical analysis

To evaluate the *in vivo* correlation between CEST and MRS results, we employed linear correlation, calculating the Pearson correlation coefficient for both the CEST MTR asymmetry and AREX values, along with the metabolite concentrations obtained through MRS. For significance inspection we performed a Student *t*-test, setting the significance threshold at $p < 0.05$. Statistics were performed in R version 4.1.2 (R Core Team, 2021).

3 | RESULTS

3.1 | Simulations

Figure 1 illustrates the results of five-pool model simulations from CEST at 2 ppm for concentrations similar to those found in the human brain (10 mM) while taking the hardware limitations into account. The simulations showed that maximum CEST at 2 ppm value can be obtained with a t_{sat} of 1.5 s and a B_1rms of 2.5 μT or a t_{sat} of 1 s and a B_1rms of 3 μT. The areas in white on the right-hand side of each map represent the acquisition parameter combinations that are not possible to achieve due to SAR and hardware limitations when imaging *in vivo*. In Figure S1A we show

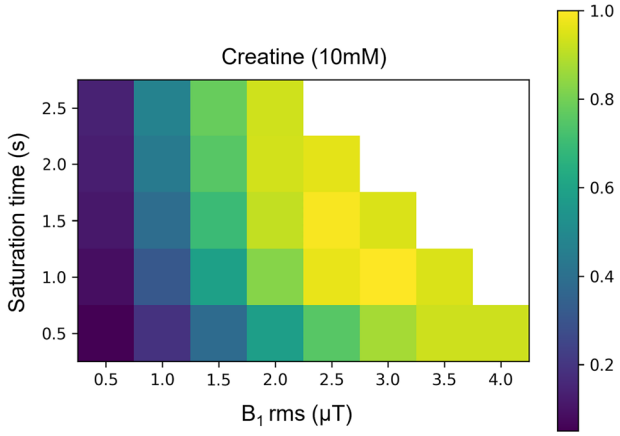

FIGURE 1 Normalized five-pool model simulation results. CEST MTR asymmetry was investigated as a function of B_1rms and t_{sat} to find the optimal acquisition values for CEST at 2 ppm CEST, corresponding to the CEST pools at 2 ppm. The areas in white on the right-hand side of each figure represent the parameter combinations that were not examined due to SAR limitations *in vivo*.

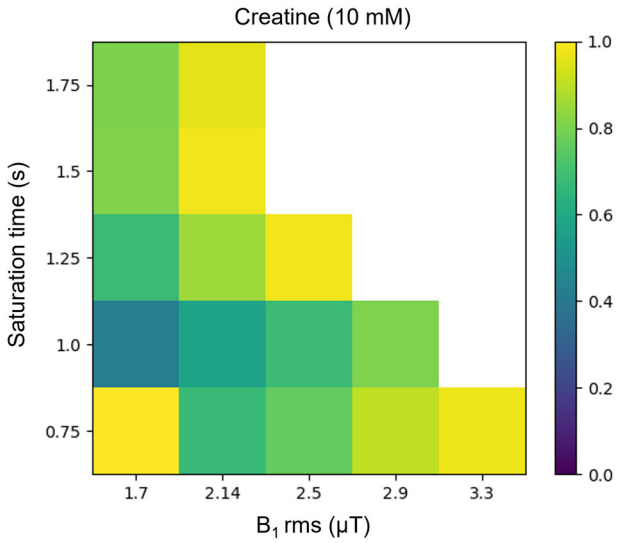

FIGURE 2 Phantom results normalized to the highest MTR asymmetry value. Maps illustrating how CEST at 2 ppm CEST changes as a function of total saturation time (s) and B_1rms (μT). The data shown corresponds to measurements of phantoms with a concentration of 10 Mm creatine scanned at ±36 °C.

that, in comparison with CEST at 2 ppm, CEST at 3 ppm requires the maximum B_1rms possible, which was approximately 3.5 μT, and a somewhat shorter t_{sat} of 1 s.

3.2 | Phantoms

Figure 2 illustrates how CEST at 2 ppm changes in vitro at 36 °C as a function of t_{sat} and B_1rms. Results at other temperatures can be found in Figure S3. We wanted to specifically assess the optimal parameters to achieve maximum CEST contrast in an ideal experimental setting before applying it *in vivo*. Our results confirm that maximum CEST at 2 ppm was reached when using a $t_{sat} = 1500$ ms and a B_1rms of 2.14 μT. Unexpectedly, a t_{sat} of 750 ms and a B_1rms of 1.7 μT also yielded maximum CEST at 2 ppm. For CEST at 3 ppm, similarly to the literature, we found that a t_{sat} of 750 ms and a B_1rms of 3.3 μT yielded the maximum MTR asymmetry (Figure S1B). Additionally, we found temperature to have a linear relation with CEST at 2 ppm MTR asymmetry, where a physiological temperature yielded higher CEST contrast than did room temperature (Figure S3A). Interestingly, for CEST at 3 ppm MTR asymmetry we observed the opposite: an inverse relation between temperature and MTR asymmetry (Figure S3B).

3.3 | Healthy volunteers

Figure 3 shows a representative example of how the MRS VOIs were planned in the GM and WM. The corresponding MR spectra are displayed for each VOI alongside the fitted signals of interest: tCr and Glu. Both metabolites could be measured and the results presented here represent reflect the average findings from all included subjects: similar concentrations of tCr in WM (VOI1, 6.6 mM ± 0.4; VOI2, 6.6 mM ± 0.3) and GM (VOI3, 6.6 ± 0.7; VOI4, 6.6 mM ± 0.5), and a higher concentration of Glu in the GM (VOI3, 8.7 mM ± 0.7; VOI4, 8.3 mM ± 0.6) compared with the WM (VOI1, 6.5 mM ± 0.3; VOI2, 6.4 mM ± 0.6).

Figure 4 shows the average *Z*-spectra and MTR asymmetry of CEST at 2 ppm of the voxels within the MRS VOI1 and VOI2 in the WM and VOI3 and VOI4 in the GM. The MTR asymmetry peak appears to be more evident in the GM voxels, whereas in the WM there seems to be a greater contribution from NOE.

CEST maps at 2 ppm are displayed in Figure 5 for two representative subjects, with respective B_0 and B_1 maps. CEST at 2 ppm maps generally exhibit high values, especially in the GM, whereas susceptibility to B_1 inhomogeneity resulted in a loss of contrast in the anatomical right side of the brain. This phenomenon appears consistent across different subjects (Figure 5A,B). In contrast, we observed a more homogeneous B_1 distribution in the CEST at 3 ppm maps (Figures S5A and S5B). Figures S7A and S7B show AREX maps from CEST at 2 ppm, where higher values can be observed in the WM compared with the GM, as AREX represents an inverse metric of steady-state *Z*-spectra.

For both MTR asymmetry and AREX, CEST at 2 ppm value distributions from all 10 subjects are displayed for the VOIs placed in the WM and in the GM in Figure 6A,B and Figure S8, respectively. CEST at 2 ppm MTR asymmetry values are broadly distributed, mostly between 0% and 20% in both GM and WM VOIs, whereas the AREX values range between 0% and 80%. CEST at 3 ppm MTR asymmetry is mostly distributed between −10% and 5% in the WM and tends toward higher values in the GM (−10% to 10%) (Figure 6C,D). Intra-tissue distribution variability (i.e., VOI1 versus VOI2 or VOI3 versus VOI4) is observed for both CEST pools, for both CEST at 2 ppm and CEST at 3 ppm distributions in the GM and WM, with slightly less variation for CEST at 3 ppm contrast in the WM (Figure 6C).

Figure 7A,B demonstrates the correlation between metabolite concentrations measured in the GM and WM and the corresponding CEST at 2 ppm MTR asymmetry values. Figure 7A shows a nonsignificant correlation between tCr and CEST at 2 ppm contrast ($R = 0.19$; $p = 0.273$). However, in Figure 7B a significant correlation was found between CEST at 2 ppm and Glu concentration ($R = 0.39$; $p = 0.033$). We conducted similar comparisons for the AREX, an inverse metric of the *Z*-spectra, which also accounts for MT and T_1. In Figure 7C,D, similarly to MTR

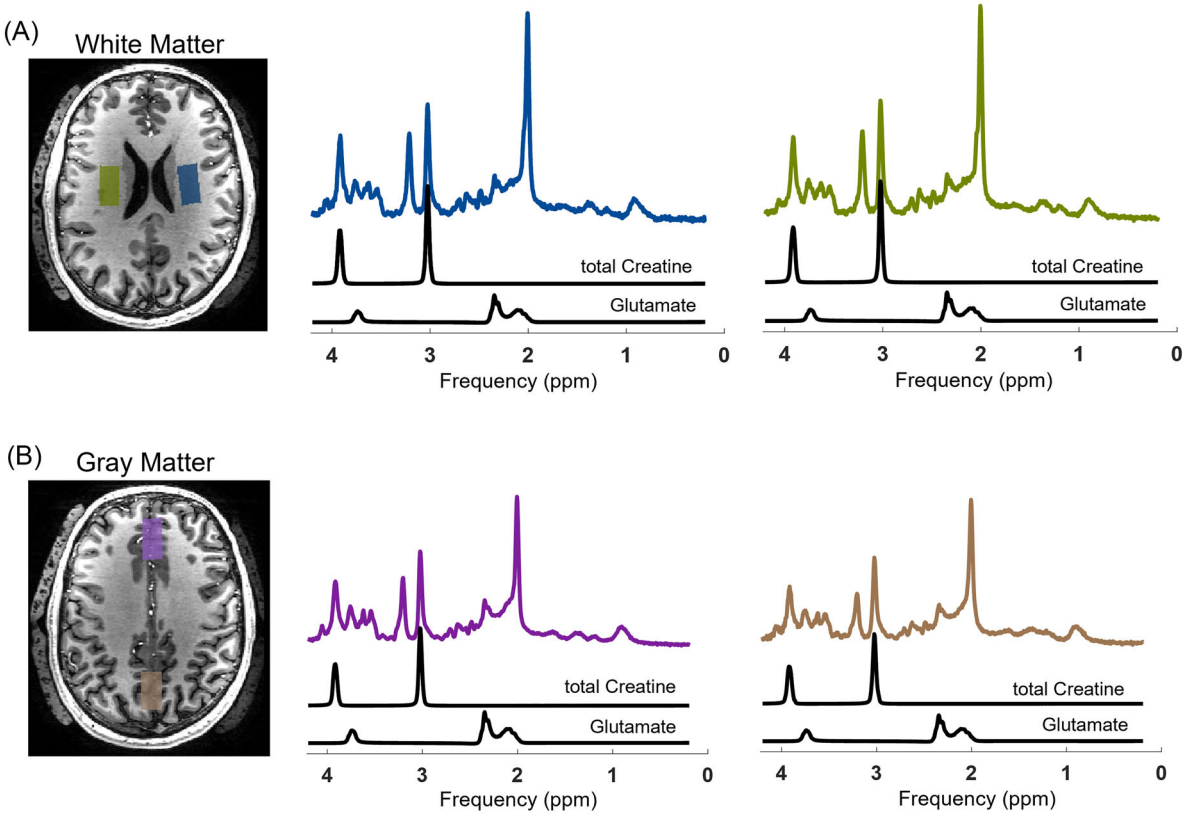

FIGURE 3 An example of how the MRS VOIs were planned, and typical MRS results showing tCr and Glu fits from the WM (A) and from the GM (B). Outside of the skull area the dielectric pads can be seen.

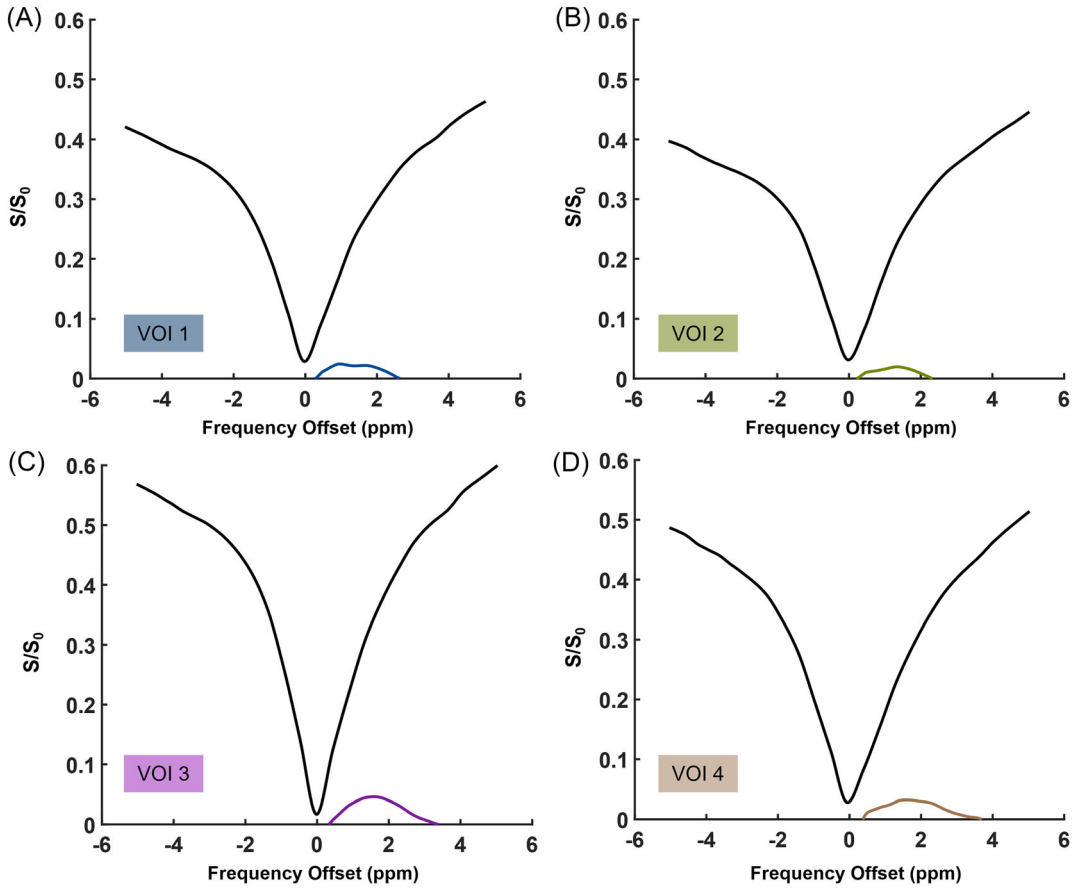

FIGURE 4 Average Z-spectra and MTR asymmetry of the voxels in two VOIs in the WM (A, B) and GM (C, D). These results are from one representative volunteer.

asymmetry results, we found no correlation of AREX at 2 ppm and tCr ($R = 0.003$; $p = 0.98$) but an inverse significant correlation between AREX at 2 ppm and Glu ($R = 0.6$; $p = 0.002$). For internal validation, we also confirmed the significant correlation between the CEST at 3 ppm MTR asymmetry and Glu concentration ($R = 0.66$; $p < 0.001$) and did not find a significant correlation between CEST at 3 ppm MTR asymmetry and tCr ($R = 0.07$; $p = 0.681$) (Figure S6A,B, respectively). Similarly, no correlation between CEST at 3 ppm and tCr was obtained using the AREX metric; however, also in this case, an inverse significant correlation between AREX at 3 ppm and Glu was obtained ($p = 0.010$; $R = 0.47$) (Figures S6C,D).

4 | DISCUSSION AND CONCLUSIONS

The primary objective of our study was to further investigate CEST at 2 ppm in the human brain at 7 T. Additionally, we conducted an internal validation of CEST at 3 ppm on a 7 T human MR platform different from that predominantly used in previous studies in the literature. First, we identified optimal CEST at 2 ppm acquisition parameters in the human brain at 7 T through simulations and confirmed them in phantoms in vitro. Subsequently, we evaluated the performance of the optimized sequences in the *in vivo* human brain using MRS as ground truth measurements of tCr and Glu concentrations. Our findings revealed a significant correlation between CEST at 2 ppm MTR asymmetry and Glu as measured by MRS, suggesting that Glu is a substantial contributor to the observed CEST at 2 ppm contrast in the human brain. However, we did not observe a significant correlation between CEST at 2 ppm and Cr concentration in the brain.

Glu-weighted CEST imaging in the brain is gaining attention given its abundance and physiological role, supported by its visibility due to the presence of amine protons.[13] Because of the involvement of Glu in pathologies such as epilepsy, the use of CEST for Glu imaging at 7 T has been explored in at least three previous studies.[7,8,29] Similarly, Cr is well known for playing an important role in tissue bioenergetics and is present in both muscles and brain, aiding in adenosine triphosphate synthesis for cell energy requirements.[30] Cr, with its amine and guanidinium protons, is an interesting CEST contrast to explore in *in vivo* human brain, especially considering its observed concentration changes in brain tumors.[31] Although both metabolites have amine protons, amines found in Glu resonate around 3 ppm from water with an exchange rate of approximately

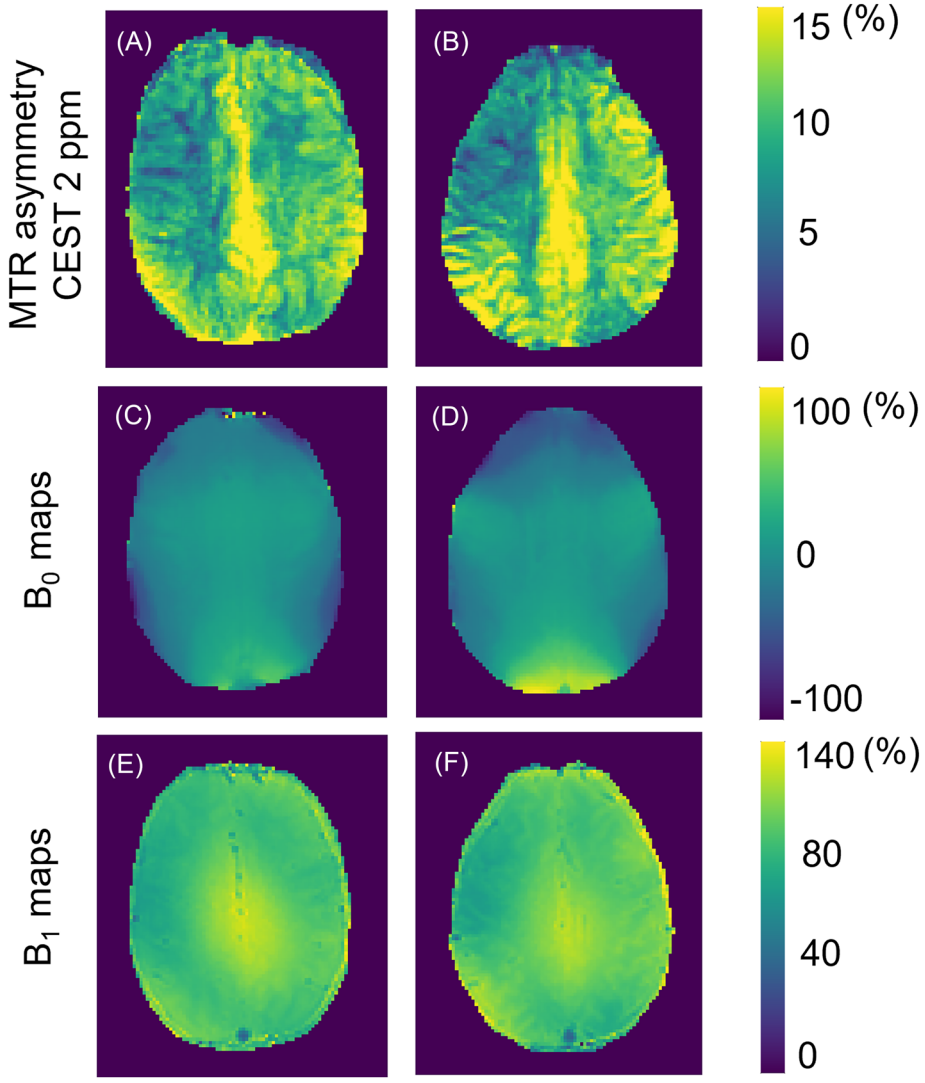

FIGURE 5 A, B, CEST at 2 ppm MTR asymmetry maps of two representative subjects. C, D, and E, F, the corresponding B_0 and B_1 maps, respectively.

5500 ± 500 Hz (Reference 13), while amines in Cr resonate around 2 ppm with an intermediate exchange rate of around 950 ± 100 Hz (Reference 17). Their neighboring frequencies and the overlap between these two pools create a challenge of specificity to each pool. Nevertheless, by taking advantage of the inherent differences in the exchange rates of amines in Glu and Cr, we determined via simulations the optimal saturation length and power to achieve maximum saturation efficiency for the two metabolites separately, while accounting for SAR and hardware limitations of human MRI scanners. Consistent with a previous study, our simulation results (Figure 1) showed that an intermediate B_1rms with a long t_{sat} is essential to achieve maximum CEST at 2 ppm MTR asymmetry contrast. In the case of CEST at 3 ppm, our results corroborated previous findings on a human 7 T system from a different vendor, emphasizing the need for a high B_1rms with a shorter t_{sat} to achieve high CEST at 3 ppm contrast.[10,13,15]

Via in vitro experiments, we validated the simulation results and determined the optimal RF power (B_1rms) and t_{sat} length to be 2.14 μT and 1500 ms and 3.3 μT and 1000 ms for CEST at 2 ppm and CEST at 3 ppm, respectively (Figures 2 and S1B, respectively). While one might argue, based on MTR asymmetry results (Figure 1), that choosing a higher B_1rms would be beneficial for CEST at 2 ppm, our assessment with the presence of Glu, as expected in the human brain, revealed that a B_1rms of 2.5 μT and a t_{sat} of 1500 ms, would noticeably increase the contribution of CEST at 3 ppm (Figure S2A). Interestingly, a considerably high CEST MTR asymmetry was found in our phantoms with a low t_{sat} and B_1rms (750 ms and 2.5 μT) (Figure 2). This observation, which is not supported by our simulations, could be attributed to field inhomogeneities, possibly induced by the movement of water within the heating blanket used during our measurements. Interestingly, a previous study that looked at CEST at 2 ppm fittings in the human brain showed a somewhat lower B_1rms of 1.45 μT and a slightly longer saturation duration of 2 s to be more beneficial for CEST at 2 ppm imaging.[14] However, the same study indicated that a B_1rms of 2 μT and total saturation of 2 s yielded CEST at 2 ppm

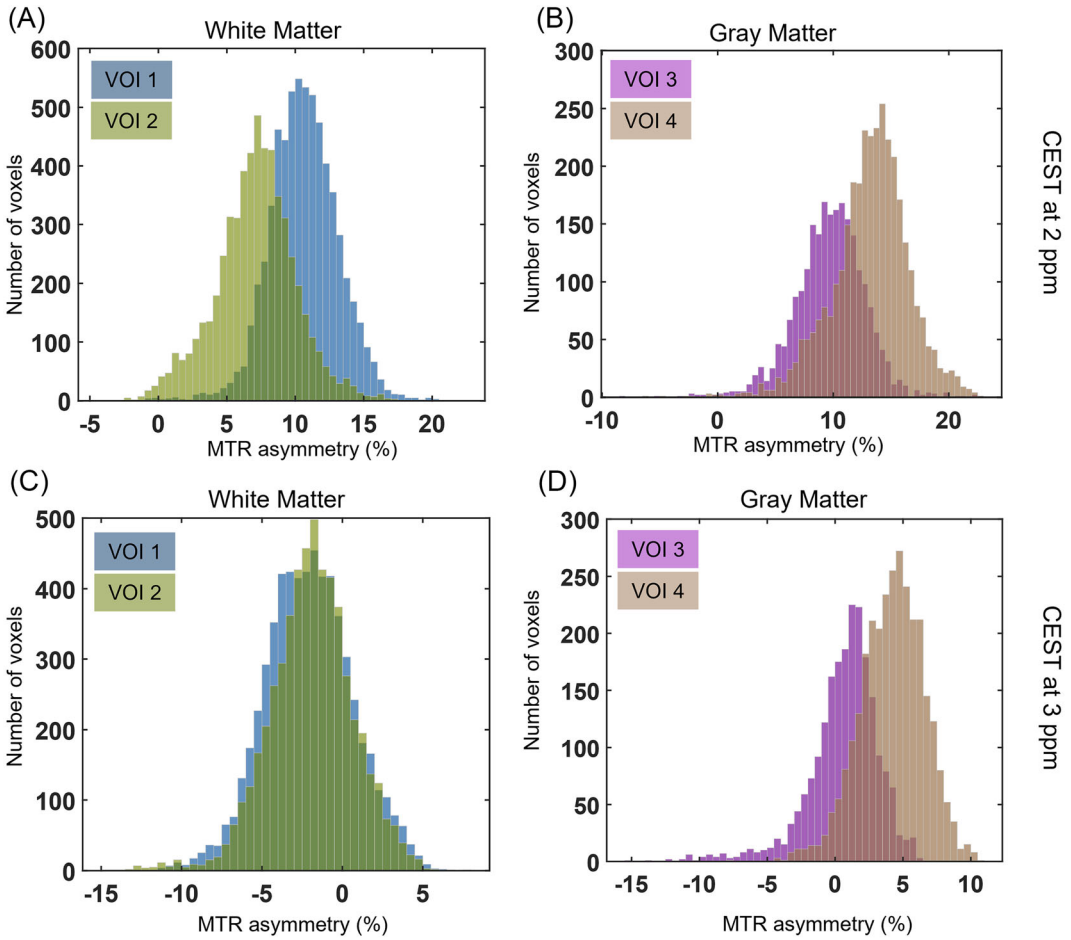

FIGURE 6 Histograms of the CEST MTR asymmetry contrast distribution from CEST at 2 ppm (A, B) and CEST at 3 ppm (C, D) in the VOIs placed in WM and GM, respectively. For each VOI the histogram reflects the average contrast across all eight imaging slices from the 10 subjects combined.

contrast comparable to that for their suggested parameters (approximately 5% in the GM). Our simulation results did initially show the benefit of aiming for a slightly higher B_1rms of 2.5 or 3 μT, with t_{sat} set at either 1 or 1.5 s, respectively. This is different from what we observed in phantoms, where the optimal acquisition parameters were first a B_1rms of 2.14 μT with a t_{sat} of 1.5 s, and second a B_1rms of 2.5 μT with a t_{sat} of 1.25 s. The latter B_1rms is in line with what has been also recently shown to be optimal for CrCEST imaging in the mouse brain.[15] As for CEST at 3 ppm, the highest B_1rms of 3.3 μT with a t_{sat} of 1000 ms could not be reached within the SAR limitations. Consequently, for phantom experiments, we chose to reduce t_{sat} to 750 ms and found the highest t_{sat} possible to be 750 ms while accommodating a B_1rms of 3.3 μT. In vitro studies in our work showed that the CEST contrasts at 2 and 3 ppm both increased with an increase in concentration (Figure S3). Phantom experiments to validate metabolite-weighted contrast have been previously performed by Khlebnikov et al.[10] In contrast to that work, our conclusions are also based on *in vivo* experiments. Our results indicate that hardware limitations need to be taken into account when developing and optimizing acquisition parameters, and emphasize the importance of choosing a concentration representative of physiological conditions to accurately mimic *in vivo* situations.

To study the metabolite-weighted CEST contrast in the human brain, we applied CEST measurements using the optimized acquisition parameters and validated them against MRS. While many prior studies have applied specific CEST sequences to capture CEST at 3 ppm contrast, we have also included MRS for validation of CEST at 2 ppm in the GM and WM of multiple subjects, in addition to what has been previously done.[14] As expected, our results showed a significant correlation between Glu concentrations and CEST at 3 ppm MTR asymmetry (Figure S6B). Surprisingly, we observed a significant correlation between CEST at 2 ppm and Glu concentrations, whereas no correlation was found between CEST at 2 ppm and tCr concentrations. The lack of correlation for CEST at 2 ppm could be attributed to different reasons. First, the well known similarity in Cr concentrations in the GM and WM limits the range over which the correlation could be assessed.[32] A potential future approach could include measurements in physiological conditions, such as during muscle exercise, where more pronounced tCr concentration changes are expected. Additionally, MRS measures tCr, therefore the phosphocreatine also contributes to the MRS measurements. The CEST contrast at

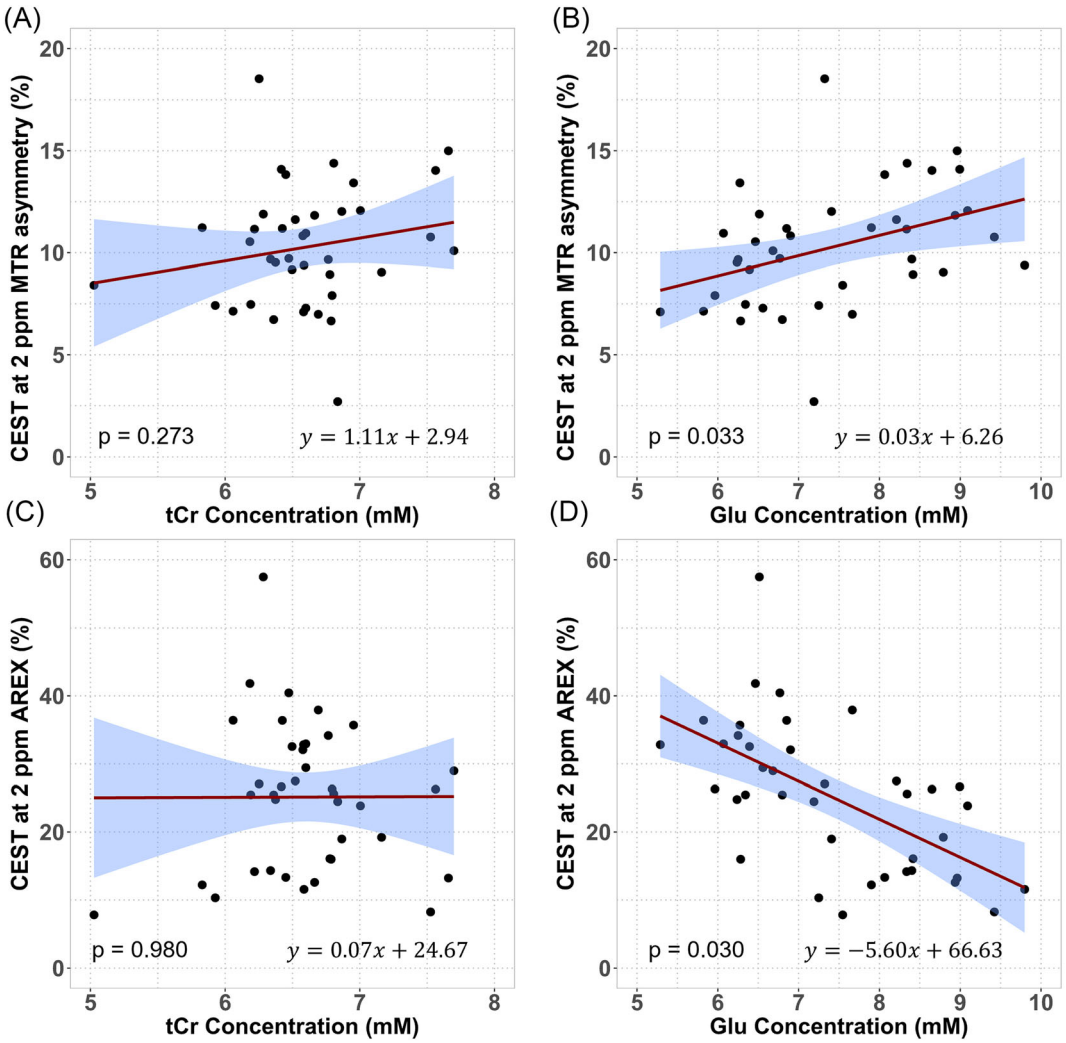

FIGURE 7 *In vivo* correlation results from data acquired with B_1rms = 2.14 μT: correlations of the MTR asymmetry (A, B) ($p = 0.273$, $p = 0.033$) and AREX (C, D) ($p = 0.980$, $p = 0.030$) of CEST at 2 ppm with tCr and Glu concentrations measured with MRS, respectively. The data plotted correspond to 39 VOIs in both GM and WM as measured in 10 subjects.

2 ppm is known to have a PCr contribution around 80% in the rat brain with a saturation of 2 μT.[33,34] Although we know that the concentrations of Cr and PCr are comparable in magnitude in the human brain, we do not know in which proportions we are capturing the signal from Cr and/or PCr.[35] Differences in relative sensitivity to Cr and PCr could potentially play a role in correlating results from these two methodologies. Finally, the CEST contribution at 2 ppm can also include contrast from other proteins/peptides, from which some guanidinium protons contribution can arise, as previously shown by Zhang et al.[33] On the other hand, the correlation of the CEST at 2 ppm pool with Glu concentrations could be due to contamination from the CEST at 3 ppm pool. It is known that this CEST pool can have a broad effect, especially at physiological temperatures. Moreover, Glu concentrations in the brain are higher than those of tCr, making it relatively easier to be more sensitive to the proton pool at 3 ppm. These results seem to suggest that the CEST MTR asymmetry contrast at 2 ppm is significantly influenced by Glu. On the other hand, when quantifying CEST with AREX, thus correcting for T_1 and MT effects, we found similar results for both CEST at 2 ppm and CEST at 3 ppm compared with MTR asymmetry (Figure 7 and Figure S6). The observed inverse correlations were expected, as the AREX calculates the inverse Lorentzian difference.[36] The inverse CEST effect can also be seen in Figure S7, where the WM appears more hyperintense than the GM, contrary to what we observed in MTR asymmetry maps (Figure 6A,B).

Previous studies have shown the feasibility of CEST at 3 ppm imaging in the human brain at 7 T.[4,13] Through simulations, in vitro experiments and measurements in healthy volunteers, we confirmed that the previously employed acquisition parameters also work on a 7 T platform different from that used predominantly in the literature from a single center. By correlating the CEST at 3 ppm MTR asymmetry values with Glu concentrations, we can confirm that Glu is a substantial contributor to the CEST at 3 ppm contrast. Interestingly, a recent study has challenged the origins

of the CEST contrast at 3 ppm, suggesting that it arises mainly from proteins rather than Glu in the rat brain.[12] Despite the difference in species, it is important to note that the data were acquired at a field strength higher than typically used in studies involving human subjects. Notably, the employed B_1 power was similar to our settings at 7 T (3.6 μT), whereas previous simulations have shown that to achieve sensitivity to Glu at 9.4 T a B_1 of around 7.5 μT would be optimal.[10] Additionally, simulations suggest that the CEST peak at 3 ppm becomes wider with increased B_0.[2] Consequently, the CEST contrast of proteins, which is typically observed around 3.5 ppm at 3 and 7 T, might have also contributed to the observed effects around 3 ppm in that particular study.

When comparing the CEST contrast distributions within the two VOIs representing WM and GM for CEST at 2 ppm (Figure 6A,B), or even for CEST at 3 ppm (Figure 6C,D), the interregional spread is evident. These differences might be attributable to discrepancies in B_1 distribution within the brain illustrated in Figure 5E,F (or Figure S5E,F), even though for the vast majority of VOIs the B_1 was above 80% (Table S3). The B_1 differences predominantly appear as the systematic right–left variation, which reflect intraregional MTR asymmetry distribution in the WM VOIs (Figure 6A,C). We attempted to mitigate B_1 inhomogeneity effects by using dielectric pads during data acquisition and by applying a quadratic B_1 correction method.[23] The fact that the B_1 correction approach was originally developed for CEST at 3 ppm, which in principle uses a higher B_1 power value, might explain why it did not perform as effectively for the CEST at 2 ppm data. Furthermore, the uneven histogram distribution and negative values in WM could also be explained by contribution of other CEST effects such as MT and NOE to the MTR asymmetry. We would expect for the most part less contamination, especially when acquiring images with higher B_1rms (i.e., filtering out other competing effects from slower exchanging pools such as NOE and amide protons). However, imperfect saturation and B_1 homogeneity distribution *in vivo* might have led to contamination to some extent throughout data acquisition, becoming more noticeable when combining data from all volunteers. Other analysis methods such as Lorentzian fittings could be considered as a good alternative for filtering out prominent competing effects *in vivo*.[37,38] After performing these fits, we computed the AREX metric accounting for T_1 and MT, but still observed an uneven distribution of the CEST contrast (Figure S8). This could perhaps be due to field inhomogeneities, or challenges arising from fitting broad CEST pools. Consequently, contamination by neighboring pools may result in the interference of undesired CEST effects, as exemplified in one volunteer in Figure S7. Our results in Figure S9 show how broad the CEST at 2 ppm and CEST at 3 ppm fittings are within the frequency spectrum, in line with a previous observation that the CEST contrast from fast exchanging components does not follow a Lorentzian line shape.[39] This has also been previously described in literature suggesting[40,41] that, because of the rather wide CEST at 3 ppm effect at physiological pH, fitting Lorentzians is particularly challenging because of the very wide peak.[40] Xu et al. state that the specificity of performing Lorentzian fittings improves CEST at 2 ppm quantification and that Cr and PCr pools could be extracted from animal muscle.[34] However, the concentration of these metabolites in muscle is higher than in the brain, and studies supporting this claim have been conducted at 11.7 T, allowing for a higher spectral resolution than at 7 T.[41–43]

In addition to the B_1 inhomogeneities, our study has a few other limitations. An interesting cofounder affecting in vitro experiments for CEST at 3 ppm contrast seems to be temperature. We observed CEST at 2 ppm and CEST at 3 ppm contrasts to have a linear and inverse relation with temperature, respectively (Figure S3B), as also shown in a zebrafish model for CEST at 3 ppm.[44] Finally, since this investigation primarily served as a proof of principle for CEST at 2 ppm, our conclusions are limited by the relatively small sample size of 10 subjects, all of whom were healthy. However, the subjects spanned a relatively wide age range, which might have helped to study the CEST contrasts over different metabolite concentrations, since it is known that metabolite concentration in the brain changes with age.[45]

In conclusion, we investigated optimal acquisition parameters for metabolite CEST imaging through simulations and validated these concepts in a controlled in vitro environment. We confirmed the significant contribution of Glu to the CEST at 3 ppm MTR asymmetry *in vivo*. Contrary to expectations, we observed that the CEST at 2 ppm pool is significantly correlated with Glu concentrations, indicating that the contrast is likely weighted by Glu. Our findings suggest that Glu is a substantial contributor to the CEST at 2 ppm contrast observed in the human brain, whereas the Cr contribution to CEST at 2 ppm in the brain did not exhibit a significant impact. A potentially interesting future step could involve applying a similar protocol in muscle imaging to assess whether CEST at 2 ppm can be validated in the presence of a larger concentration of Cr protons. Furthermore, it would be valuable to verify these sequences in pathologies such as brain tumors, expanding on the work of Cai et al.[46] This way, the specificity of metabolite-weighted CEST could be reliably validated for future clinical applications.

ACKNOWLEDGMENTS

This study is part of "Non-Invasive Characterization of Active Multiple Sclerosis Lesions Through Chemical Exchange Saturation Transfer (CEST) Imaging" (Project 16862) financed by the Dutch Research Council (NWO) Talent Programme Veni. This work was also funded by the Medical Delta Cancer Diagnostics 3.0 program.

We would like to thank Wyger Brink for making the dielectric pads we used and supporting us while tackling B_1 constraints during protocol optimization. We would also like to thank Emiel C.A. Roefs for support while fine-tuning the analysis pipeline and with adjusting the T_1 and T_2 of the phantoms.

CONFLICT OF INTEREST STATEMENT

Ece Ercan is a full-time employee at Philips Healthcare, Best, The Netherlands.

ORCID

Bárbara Schmitz-Abecassis https://orcid.org/0000-0003-1776-4560

Chloé Najac https://orcid.org/0000-0002-7804-2281

Matthias J. P. van Osch https://orcid.org/0000-0001-7034-8959

Ece Ercan https://orcid.org/0000-0002-8187-2075

REFERENCES

1. van Zijl PCM, Yadav NN. Chemical exchange saturation transfer (CEST): what is in a name and what isn't? *Magn Reson Med*. 2011;65(4):927-948. doi:10.1002/mrm.22761
2. van Zijl PCM, Lam WW, Xu J, Knutsson L, Stanisz GJ. Magnetization transfer contrast and chemical exchange saturation transfer MRI. Features and analysis of the field-dependent saturation spectrum. *NeuroImage*. 2018;(168):222-241. doi:10.1016/j.neuroimage.2017.04.045
3. Haris M, Nanga RPR, Singh A, et al. Exchange rates of creatine kinase metabolites: feasibility of imaging creatine by chemical exchange saturation transfer MRI. *NMR Biomed*. 2012;25(11):1305-1309. doi:10.1002/nbm.2792
4. Cai K, Singh A, Roalf DR, et al. Mapping glutamate in subcortical brain structures using high-resolution GluCEST MRI. *NMR Biomed*. 2013;26(10):1278-1284. doi:10.1002/nbm.2949
5. Kogan F, Harris M, DeBrosse C, et al. In vivo CEST imaging of creatine (CrCEST) in skeletal muscle at 3T. *J Magn Reson Imaging*. 2014;40(3):596-602. doi:10.1002/jmri.24412.In
6. Kogan F, Haris M, Singh A, et al. Method for high-resolution imaging of creatine in vivo using chemical exchange saturation transfer. *Magn Reson Med*. 2014;71(1):164-172. doi:10.1002/mrm.24641
7. Davis KA, Nanga RPR, Das S, et al. Glutamate imaging (GluCEST) lateralizes epileptic foci in nonlesional temporal lobe epilepsy. *Sci Transl Med*. 2015;7(309):309ra161. doi:10.1126/scitranslmed.aaa7095
8. Neal A, Moffat BA, Stein JM, et al. Glutamate weighted imaging contrast in gliomas with 7 Tesla magnetic resonance imaging. *NeuroImage Clin*. 2019;22:101694. doi:10.1016/j.nicl.2019.101694
9. Cai K, Wen TR, Zhou XJ, et al. Creatine CEST MRI for differentiating gliomas with different degrees of aggressiveness. *Mol Imaging Biol*. 2018;19(2):225-232. doi:10.1007/s11307-016-0995-0.Creatine
10. Khlebnikov V, van der Kemp WJM, Hoogduin H, Klomp DWJ, Prompers JJ. Analysis of chemical exchange saturation transfer contributions from brain metabolites to the Z-spectra at various field strengths and pH. *Sci Rep*. 2019;9(1):1089. doi:10.1038/s41598-018-37295-y
11. Goerke S, Zaiss M, Bachert P. Characterization of creatine guanidinium proton exchange by water-exchange (WEX) spectroscopy for absolute-pH CEST imaging in vitro. *NMR Biomed*. 2014;27(5):507-518. doi:10.1002/nbm.3086
12. Cui J, Zu Z. Towards the molecular origin of glutamate CEST (GluCEST) imaging in rat brain. *Magn Reson Med*. 2020;83(4):1405-1417. doi:10.1002/mrm.28021
13. Cai K, Haris M, Singh A, et al. Magnetic resonance imaging of glutamate. *Nat Med*. 2012;18(2):302-306. doi:10.1038/nm.2615.Magnetic
14. Singh A, Debnath A, Cai K, et al. Evaluating the feasibility of creatine-weighted CEST MRI in human brain at 7T using a Z-spectral fitting approach. *NMR Biomed*. 2019;32(12):e4176. doi:10.1002/nbm.4176
15. Zhang Z, Wang K, Park S, et al. The exchange rate of creatine CEST in mouse brain. *Magn Reson Med*. 2023;2:373-384. doi:10.1002/mrm.29662
16. Zaiss M, Zu Z, Xu J, et al. A combined analytical solution for chemical exchange saturation transfer and semi-solid magnetization transfer. *NMR Biomed*. 2015;28(2):217-230. doi:10.1002/nbm.3237.A
17. Mueller S, Scheffler K, Zaiss M. On the interference from agar in chemical exchange saturation transfer MRI parameter optimization in model solutions. *NMR Biomed*. 2021;34(1):e4403. doi:10.1002/nbm.4403
18. Kim M, Gillen J, Landman BA, Zhou J, van Zijl PCM. Water saturation shift referencing (WASSR) for chemical exchange saturation transfer (CEST) experiments. *Magn Reson Med*. 2009;61(6):1441-1450. doi:10.1002/mrm.21873
19. Teeuwisse WM, Brink WM, Webb AG. Quantitative assessment of the effects of high-permittivity pads in 7Tesla MRI of the brain. *Magn Reson Med*. 2012;67(5):1285-1293. doi:10.1002/mrm.23108
20. O'Reilly TPA, Webb AG, Brink WM. Practical improvements in the design of high permittivity pads for dielectric shimming in neuroimaging at 7T. *J Magn Reson*. 2016;270:108-114. doi:10.1016/j.jmr.2016.07.003
21. Smith SM. Fast robust automated brain extraction. *Hum Brain Mapp*. 2002;17(3):143-155. doi:10.1002/hbm.10062
22. Zhang Y, Brady M, Smith S. Segmentation of brain MR images through a hidden Markov random field model and the expectation-maximization algorithm. *IEEE Trans Med Imaging*. 2001;20(1):45-57. doi:10.1109/42.906424
23. Singh A, Cai K, Haris M, Hariharan H, Reddy R. On B1 inhomogeneity correction of in vivo human brain glutamate chemical exchange saturation transfer contrast at 7T. *Magn Reson Med*. 2013;69(3):818-824. doi:10.1002/mrm.24290
24. Windschuh J, Zaiss M, Meissner JE, et al. Correction of B1-inhomogeneities for relaxation-compensated CEST imaging at 7T. *NMR Biomed*. 2015;28(5):529-537. doi:10.1002/nbm.3283
25. Zaiss M, Windschuh J, Paech D, et al. Relaxation-compensated CEST-MRI of the human brain at 7T: unbiased insight into NOE and amide signal changes in human glioblastoma. *NeuroImage*. 2015;112:180-188. doi:10.1016/j.neuroimage.2015.02.040
26. Provencher SW. Estimation of metabolite concentrations from localized in vivo proton NMR spectra. *Magn Reson Med*. 1993;30(6):672-679. doi:10.1002/mrm.1910300604
27. Simpson R, Devenyi GA, Jezzard P, Hennessy TJ, Near J. Advanced processing and simulation of MRS data using the FID appliance (FID-A)—an open source, MATLAB-based toolkit. *Magn Reson Med*. 2017;77(1):23-33. doi:10.1002/mrm.26091
28. Marjańska M, Auerbach EJ, Valabrègue R, Van de Moortele PF, Adriany G, Garwood M. Localized 1H NMR spectroscopy in different regions of human brain in vivo at 7T: T2 relaxation times and concentrations of cerebral metabolites. *NMR Biomed*. 2012;25(2):332-339. doi:10.1002/nbm.1754
29. Lucas A, Nanga RPR, Hadar P, et al. Mapping hippocampal glutamate in mesial temporal lobe epilepsy with glutamate weighted CEST (GluCEST) imaging. *Hum Brain Mapp*. 2022;2:549-558. doi:10.1002/hbm.26083
30. Belitzer WA, Golovskaya KS. Phosphate acceptors in "respiratory phosphorylation" in muscle tissue. *Science*. 1940;92(2397):536-537.

31. Li X, Lu Y, Pirzkall A, McKnight T, Nelson SJ. Analysis of the spatial characteristics of metabolic abnormalities in newly diagnosed glioma patients. *J Magn Reson Imaging*. 2002;16(3):229-237. doi:10.1002/jmri.10147
32. Schuff N, Ezekiel F, Gamst AC, et al. Region and tissue differences of metabolites in normally aged brain using multislice 1H magnetic resonance spectroscopic imaging. *Magn Reson Med*. 2001;45(5):899-907. doi:10.1002/mrm.1119
33. Zhang XY, Xie J, Wang F, et al. Assignment of the molecular origins of CEST signals at 2 ppm in rat brain. *Magn Reson Med*. 2017;78(3):881-887. doi:10.1002/mrm.26802
34. Xu J, Chung JJ, Jin T. Chemical exchange saturation transfer imaging of creatine, phosphocreatine, and protein arginine residue in tissues. *NMR Biomed*. 2023;36(6):e4671. doi:10.1002/nbm.4671
35. Duarte JMN, Lei H, Mlynárik V, Gruetter R. The neurochemical profile quantified by in vivo 1H NMR spectroscopy. *NeuroImage*. 2012;61(2):342-362. doi:10.1016/j.neuroimage.2011.12.038
36. Jones CK, Huang A, Xu J, et al. Nuclear Overhauser enhancement (NOE) imaging in the human brain at 7T. *NeuroImage*. 2013;77:114-124. doi:10.1016/j.neuroimage.2013.03.047
37. Zaiß M, Schmitt B, Bachert P. Quantitative separation of CEST effect from magnetization transfer and spillover effects by Lorentzian-line-fit analysis of z-spectra. *J Magn Reson*. 2011;211(2):149-155. doi:10.1016/j.jmr.2011.05.001
38. Schmitz-Abecassis B, Vinogradov E, Wijnen JP, et al. The use of variable delay multipulse chemical exchange saturation transfer for separately assessing different CEST pools in the human brain at 7T. *Magn Reson Med*. 2022;87(2):872-883. doi:10.1002/mrm.29005
39. Zhang XY, Wang F, Li H, et al. Accuracy in the quantification of chemical exchange saturation transfer (CEST) and relayed nuclear Overhauser enhancement (rNOE) saturation transfer effects. *NMR Biomed*. 2017;30(7):e3716. doi:10.1002/nbm.3716
40. Cember ATJ, Nanga RPR, Reddy R. Glutamate weighted CEST (gluCEST) imaging for mapping neurometabolism: an update on the state of the art and emerging findings from in vivo applications. *NMR Biomed*. 2022;6:e4780. doi:10.1002/nbm.4780
41. Chung JJ, Jin T, Lee JH, Kim SG. Chemical exchange saturation transfer imaging of phosphocreatine in the muscle. *Magn Reson Med*. 2019;81(6):3476-3487. doi:10.1002/mrm.27655
42. Chen L, Zeng H, Xu X, et al. Investigation of the contribution of total creatine to the CEST Z-spectrum of brain using a knockout mouse model. *NMR Biomed*. 2018;30(12):e3834. doi:10.1002/nbm.3834.Investigation
43. Chen L, Barker PB, Weiss RG, van Zijl PCM, Xu J. Creatine and phosphocreatine mapping of mouse skeletal muscle by a polynomial and Lorentzian line-shape fitting CEST method. *Magn Reson Med*. 2019;81(1):69-78. doi:10.1002/mrm.27514.Creatine
44. Wermter FC, Bock C, Dreher W. Investigating GluCEST and its specificity for pH mapping at low temperatures. *NMR Biomed*. 2015;28(11):1507-1517. doi:10.1002/nbm.3416
45. Kakimoto A, Ito S, Okada H, Nishizawa S, Minoshima S, Ouchi Y. Age-related sex-specific changes in brain metabolism and morphology. *J Nucl Med*. 2016;57(2):221-225. doi:10.2967/jnumed.115.166439
46. Cai K, Singh A, Poptani H, et al. CEST signal at 2ppm (CEST at 2ppm) from Z-spectral fitting correlates with creatine distribution in brain tumor. *NMR Biomed*. 2015;28(1):1-8. doi:10.1002/nbm.3216

SUPPORTING INFORMATION

Additional supporting information can be found online in the Supporting Information section at the end of this article.

How to cite this article: Schmitz-Abecassis B, Najac C, Plugge J, van Osch MJP, Ercan E. Investigation of metabolite correlates of CEST in the human brain at 7 T. *NMR in Biomedicine*. 2024;e5104. doi:10.1002/nbm.5104